GEOPHYSICS, VOL. 68, NO. 5 (SEPTEMBER-OCTOBER 2003); P. 1714–1730, 14 FIGS.
10.1190/1.1620645

Inferring the statistical distribution of velocity heterogeneities by statistical traveltime tomography

Bertrand Iooss*, David Geraets‡, Tapan Mukerji**, Yann Samuelides§, Mustafa Touati§§, and Alain Galli‡‡

ABSTRACT

Understanding the internal heterogeneities of reservoirs is one of the key issues in better recovery and efficient reservoir management. Seismic data are widely used to map subsurface heterogeneities. These heterogeneities can include variations in wave velocity and rock density, which can be used to interpret variations in reservoir properties such as porosity, lithofacies, and fluids. This paper describes a statistical tomography method to infer the spatial statistics of subsurface velocity heterogeneities from seismic data. We consider an acoustic wave propagating in a medium represented as a single macromodel superimposed on statistically stationary random velocity perturbations. While the macromodel is retrieved by classical seismic methods, the picked traveltimes and their fluctuations are used to estimate the covariance function of the spatially varying velocity perturbations. We present a formulation based on ray-theoretical results and describe two algorithms: one using the prestack traveltimes and the other using the stacking velocities. The methods are tested with synthetic seismic reflection data in an idealized medium (with a Gaussian spatial covariance) and with synthetic transmission data in a more geologically realistic medium. Then, the two algorithms are applied on real data. The estimates of the spatial statistics obtained from inverting the traveltime statistics match reasonably well with the true parameters of the heterogeneous media.

INTRODUCTION

In spite of tremendous advances in seismic imaging technology, reliable delineation and mapping of subsurface heterogeneities still remains one of the key problems in reservoir and aquifer management. Well data provide the most high-resolution and direct estimates of the reservoir heterogeneities. However, these estimates are localized close to the wellbore region and contain little information about the lateral distribution of the heterogeneities, especially when the wells are sparse. Therefore, spatially exhaustive seismic data play a crucial role in delineating the heterogeneities in the interwell regions. Since these heterogeneities are often very complex, it may be impossible to characterize them deterministically in detail. Then it becomes more effective to describe the subsurface heterogeneities statistically. One of the key steps in using seismic data to estimate statistically reservoir heterogeneities is to understand the fundamental relations between seismic traveltimes and the spatial distribution of the velocity heterogeneities.

The theory of wave propagation in random media (e.g., Chernov, 1960; Rytov et al., 1987; Sato and Fehler, 1998) is particularly well suited to link traveltime statistics and velocity statistics in a rigorous physical framework. The wave velocity field is generally assumed to be a deterministic, low fluctuating trend (scales much larger than the dominant wavelength) with random heterogeneous perturbations (scales slightly larger than the wavelength). The deterministic part of the velocity is called the macromodel, while the random part is called the midscale model. The microscale heterogeneities (size smaller than the wavelength) may be taken into account using effective medium theories (Mukerji et al., 1995; Gold et al.,

Manuscript received by the Editor February 8, 2002; revised manuscript received October 14, 2002.
*Formerly Institut Français du Pétrole, Division Géophysique, 92852 Rueil-Malmaison, France; presently CEA Cadarache, DER/STR/LCFR, 13108 Saint-Paul-lez-Durance, France. E-mail: bertrand.iooss@cea.fr.
‡École des Mines de Paris, Centre de Géostatistique, 77305 Fontainebleau, France. E-mail: dgeraets@dsimprove.be.
**Stanford University, Rock Physics Laboratory, Mitchell Building, 397 Panama Mall, Stanford, California 94305. E-mail: mukerji@stanford.edu.
§Crédit Agricole Indosuez, Fixed Income Division, 9 quai du Président Paul Doumer, 92920 Paris La Défense, France. E-mail: yann.samuelides@ca-indosuez.com.
§§Formerly Scoreboard, Inc., Herndon, Virginia; presently Saudi Aramco, E&PE TD, P.O. Box 6780, Dharan 31311, Saudi Arabia. E-mail: mustafa.touati@aramco.com.
‡‡École des Mines de Paris, Centre d'Economie Industrielle, 60 boulevard Saint Michel, 75006 Paris, France. E-mail: galli@cerna.ensmp.fr.

2000). Various approximations (e.g., Born, Rytov, Markov, first-order geometrical optics, etc.) based on the smoothness and amplitude of the velocity perturbations link the statistical moments of the wavefield (amplitude and phase) to the statistical moments of the velocity. Müller et al. (1992) use first-order geometrical optics to establish results relating the spatial covariance of the slowness (reciprocal of wave velocity) heterogeneities to the covariance of the traveltime fluctuations around the mean traveltime. The effect of statistically anisotropic distributions of random heterogeneities on traveltimes has been studied by Rytov et al. (1987), Samuelides and Mukerji (1998), Samuelides (1998), and Iooss et al. (2000).

In seismology, the stochastic inverse problem, i.e, retrieving the distribution of heterogeneities (covariance, correlation lengths) from seismic waves, is well known (Aki, 1973; Flatté and Wu, 1988; Müller et al., 1992; Klimeš, 2002b). Here, we call this inversion the statistical tomography process. Roth (1997) retrieves the velocity standard deviation and isotropic correlation length from wide-angle seismic data. However, the inversion of seismic reflection data is much more complex: plane-wave hypothesis breaks down, the heterogeneities of sedimentary layers are not statistically isotropic, and wave reflection must be accounted for during the wave propagation. In this framework, restricted to constant-velocity macromodels and slightly perturbed reflectors, Touati (1996), Touati et al. (1999), Iooss (1998a), and Iooss and Galli (2000) propose a process to estimate the horizontal correlation length of velocities from the traveltime variance at constant offset. Geraets et al. (2001) and Geraets and Galli (2002) propose a more robust way to access to this information by using stacking velocities.

This paper briefly reviews and then applies the methods based on the geometrical optics approximation to estimate the anisotropic spatial velocity covariance function from observed seismic traveltimes. In the following section, we motivate our work by introducing the role of heterogeneities in reservoir characterization and the influence of midscale velocity heterogeneities in three important stages of seismic processing. In the third section, we recall some basic results about wave propagation in weakly heterogeneous random media, and we present our inversion algorithms. One of the contributions of this paper is to consider relative traveltimes which lets us take into account macromodel variations. Then we present two methods (prestack and poststack) for statistical tomography of seismic reflection data: one using prestack picked traveltimes and the other using stacking velocities. After showing numerical results on synthetic data, we finally apply the statistical tomography process to a real data case provided by ENI-Agip division. We show that for various cases we can estimate the correlation length reasonably (within 7% to 20% of errors for different cases). We conclude by describing a flowchart of the different steps involved in the prestack and poststack methods.

EFFECTS OF HETEROGENEITIES ON RESERVOIR CHARACTERIZATION AND SEISMIC PROCESSING

In the first step, we explain the main motivations to describe subsurface inhomogeneity. Estimates of reservoir heterogeneities are important inputs in developing strategies for efficient hydrocarbon recovery, production monitoring, reservoir development, and aquifer remediation. Subsurface delineation becomes especially important in heterogeneous depositional systems such as fluvial systems and deepwater clastic and turbidite reservoirs. These often have complex sand–shale distributions; conventional seismic and well-log analysis of the heterogeneities can be very uncertain. These depositional systems can be highly compartmentalized, and 50%–80% of potentially recoverable mobile oil is bypassed and left behind in conventional reservoir development strategies (Tyler and Finley, 1991). Such reservoirs are prime targets for enhanced oil recovery (EOR) programs based on careful subsurface characterization of the heterogeneities. These heterogeneities include the spatially distributed shales, sand channels, and lobes as well as the heterogeneous distribution of pore fluids such as hydrocarbons and brine within the sand bodies. Understanding the heterogeneous fluid saturation distribution is of particular importance in the proper interpretation and utilization of time-lapse 4D seismic monitoring data.

Estimating subsurface heterogeneities also plays an important role in groundwater aquifer remediation problems (Rubin et al., 1992). In such problems, the goal is to place wells that can effectively contain the spread and diffusion of contaminants through the groundwater flow system. Decisions regarding well placement depend on a proper understanding of the heterogeneous distribution of various hydrostratigraphic units and the nature of high- and low-permeability flow channels within the aquifer. Thus, a reliable characterization of the subsurface heterogeneities is needed to improve efficiency and reduce uncertainty in reservoir and aquifer management.

Another important motivation remains on the subsurface imaging, which requires an accurate knowledge of the propagation velocity of seismic waves. However, small velocity variations can have important effects on the classical steps of seismic processing: velocity analysis (stacking techniques, tomography,) and migration process. Let us briefly introduce these estimation problems and some attempts to quantify their uncertainty with the use of the velocity covariance.

Stacking velocity analysis

To estimate the stacking velocities, we generally assume a locally invariant velocity field at the scale of the acquisition layout: fitting the CMP-gathered reflection traveltimes by hyperbola does not account for the small-scale perturbations of the velocity field. We also often assume afterwards that the covariance models of the stacking velocities and the instantaneous velocity field are equivalent (Chu et al., 1994; Wook and Wenlong, 2000).

However, the difference between these two covariance models is generally significant (Touati, 1996; Geraets and Galli, 2002) because of the increased lateral continuity from the stack filter (Gibson and Levander, 1990). Geraets and Galli (2002) show that these two covariance models are linked, and that the latter can be deduced from the former, taking into account the acquisition layout. In addition, they produce an experiment to illustrate the impact of the negligence of this acquisition factor on the resulting estimation of the correlation length. For two synthetic acquisitions with different layouts (51 and 101 geophones, respectively, and a maximum offset of 500 m and 1000 m, respectively), the estimated correlation length of the stacking velocity profiles is multiplied by a factor of five, although the random velocity field (in particular, its horizontal correlation length) does not change.

Traveltime tomography

Seismic reflection tomography aims at recovering the depths of the reflectors within the subsurface and the velocity distribution between these reflectors (Bishop et al., 1985). The standard formulation of this inverse problem consists in minimizing a least-squares objective function that measures the distance between the data (the picked traveltimes on seismic sections) and the seismic response of the model (the calculated traveltimes), to recover the earth model that best fits the data (Tarantola, 1987).

When solving an inverse problem, it is essential to have some estimate of the uncertainties on the data space to avoid misinterpreting some noise as signal (Scales and Tenorio, 2001). In reflection traveltime tomography, there are many sources of uncertainty. One source is observational errors. The time sampling of the seismic traces (typically 4 ms) creates white noise in the picked times (which leads to a typical standard deviation = 1 ms). Another source is model errors—physical factors not contained in the model which have a nonnegligible contribution to the data (e.g., diffraction effects affecting traveltimes and not taken into account by ray tracing, viscoelastic dissipation effects not taken into account in purely elastic models, etc.). Parameterization errors for the reflector and velocity model representation are another source, e.g., the choice of the basis functions (polynomial, spline functions, spherical harmonics) and the model discretization (Delprat-Jannaud and Lailly, 1993).

Two questions arise: (1) How can the model uncertainties be quantified? Estimating the statistics of velocity heterogeneities not retrieved by tomography is an important step toward answering this question and the subject of this paper. (2) How can such modeling errors be incorporated into an inverse calculation? Let us recall the work of Klimeš (2002a) who introduces the medium covariance function in the traveltime inversion formulation.

Migration errors

The problem of imaging the subsurface with seismic reflection data (the migration process) is velocity field estimation. Migration consists of replacing reflectors observed in seismic time sections at their correct lateral and vertical position (Claerbout, 1985). However, deterministic methods such as velocity analysis or traveltime tomography resolve only the large-scale structure of the velocity field (Thore and Juliard, 1999; Williamson and Worthington, 1993).

In the case of the simplest migration process (constant velocity field) and by the use of first-order geometrical optics (see "Theory" following), Matheron (1991) expressess the localization errors (horizontal and vertical) as a function of the velocity perturbations in the probabilistic framework. He shows that, neglecting weak velocity fluctuations, migration errors can become important. Moreover, if the velocity field is stationary, migration errors can be estimated by the variance of the localization errors as a function of the covariance of the velocity perturbations. Touati et al. (1999) also propose to simulate migration errors knowing the covariance of the velocity perturbations. It is possible to extend the variance formula of the migration errors to the nonstationary case (Touati, 1996).

To summarize, understanding heterogeneities is important for efficient well placement and reservoir management, as well as for more reliable processing and imaging. In this paper we focus on velocity heterogeneities. Reservoir characterization requires the additional step of mapping these velocity heterogeneities to heterogeneities in reservoir properties such as porosity, sand-shale, pore fluids, etc., using rock physics transforms.

THEORY

The stochastic medium

We assume that deterministic seismic methods can adequately identify the reflectors corresponding to the layers of the macromodel. Therefore, we study the propagation within a single layer, which we model as a statistically stationary random medium. Typically, the random medium is characterized by a spatially varying slowness field:

$$n(\mathbf{r}) = \frac{1}{c_0(\mathbf{r})}[1 + \epsilon(\mathbf{r})], \tag{1}$$

where $\mathbf{r}$ is the position vector, $\epsilon(\mathbf{r})$ is a stationary fluctuation with zero mean, and $c_0(\mathbf{r})$ is the background velocity (macromodel). If ϵ is small compared to one, the velocity field writes at first order $c(\mathbf{r}) = c_0(\mathbf{r})[1 - \epsilon(\mathbf{r})]$.

Since the heterogeneity field is stationary, its spatial structure is described by the spatial covariance function $N(\mathbf{r})$, which only depends on the difference vector $\mathbf{r}_1 - \mathbf{r}_2$:

$$\langle \epsilon(\mathbf{r}_1)\epsilon(\mathbf{r}_2)\rangle = \sigma_\epsilon^2 N(\mathbf{r}_1 - \mathbf{r}_2), \tag{2}$$

where $\langle . \rangle$ denotes the expectation operator and σ_ϵ^2 is the variance of the relative slowness fluctuations. Let $\mathbf{r} = (x, y, z)$, where (x, y) are the horizontal coordinates and z is the vertical coordinate. We assume that the covariance function can be factorized as follows: $N(\mathbf{r}) = C_\epsilon(\sqrt{(x^2/a_x^2) + (y^2/a_y^2) + (z^2/b^2)})$, where C_ϵ is the standardized covariance, a_x is the horizontal correlation length, a_y is the azimuthal correlation length, and b is the vertical correlation length. This is called the geometrical anisotropy hypothesis (Chilès and Delfiner, 1999), which means that the isocovariance lines can be approximated by concentric ellipses. Here, we restrict ourselves to the statistical transverse isotropy (TI) case: $a_x = a_y = a$. In this case, $N(\mathbf{r})$ is written as in 2D media:

$$N(\mathbf{r}) = C_\epsilon\left(\sqrt{\frac{x^2}{a^2} + \frac{z^2}{b^2}}\right), \tag{3}$$

where x is the lateral distance and z the vertical one. For simplicity, we now call C_ϵ the velocity covariance and σ_ϵ^2 the variance of the velocity perturbations.

It is useful to define another length scale, the range, as the value at which the covariance is 5% of the variance. The horizontal and vertical ranges, A and B are not the same as the correlation lengths a and b used in the covariance function. The advantage of measuring the ranges instead of the correlation lengths is that the ranges are independent of the covariance model. Then the comparison between two estimates of a range is not biased by the covariance model, while the covariance models have to be the same when comparing two correlation lengths.

The types of covariance functions used in the seismological literature (Sato and Fehler, 1998) are similar to those used in geostatistics (Chilès and Delfiner, 1999), even if the terminology differs. One of the most widely used covariance functions is the Gaussian covariance $N(h) = \exp(-h^2)$, easy to manipulate analytically and leading to simplified formulas. Moreover, most of the wave simulation methods need regular velocity fluctuations, and Gaussian covariance media have very smooth heterogeneities. In the seismological context, the power spectrum model is more applicable because it describes a wide range of random models. It is defined by the K-Bessel covariance: $N(h) = [2^{1-p}/\Gamma(p)]h^p K_p(h)$, where K_p is the modified Bessel function of the second type and of order p. The exponential covariance case ($p = 0.5$, $N(h) = \exp(-h)$) models media (Figure 1) with rougher heterogeneities but slower decrease of correlation than a Gaussian medium.

Figure 2a presents a more realistic earth model generated geostatistically with well data from a West Texas oil field. An indicator simulation (Deutsch and Journel, 1992) was carried out to simulate three facies (representing good, intermediate, and poor reservoir zones) and was conditioned to facies indicators at the wells (located at the two model edges). The three facies were then populated by simulated porosity values, and the porosities were mapped to seismic P-wave velocities by velocity–porosity relations for sandstones (Han, 1986). Thus, the principal cause of the velocity heterogeneity is the heterogeneity in the reservoir facies and the corresponding porosity.

The velocity field (Figure 2a) shows a global mean of $c_0 = 4832$ m/s and a standard deviation of 15.3% (perturbation variance of $\sigma_\epsilon^2 = 0.023$). From this map, we make a structural analysis by calculating the normalized horizontal and vertical covariances of the velocity field (Figure 2b). The two covariances show a nugget effect, i.e., a discontinuity at the origin implying subresolution microstructure at scales smaller than the grid lag. In the vertical direction, the covariance has a range of $B = 65$ m (calculated by $N(B) = 5\%$). However the velocity model shows a particular anisotropy since the horizontal covariance does not converge to zero but flattens out quickly to a sill of 0.24. In geostatistics, this is called a zonal anisotropy structure, and it means the model has a nonstationary deterministic horizontal stratification (Chilès and Delfiner, 1999). Strictly speaking, the hypothesis of geometrical anisotropy is no longer valid in this case. Taking 0.24 as the limit of convergence (instead of 0), we estimate the horizontal range as $A = 170$ m ($N(A) = 5\%(1 - 0.24) + 0.24$). Then, the anisotropy ratio $\Lambda = A/B$ is approximately 2.5. Since zonal anisotropy is a common feature in many earth models, this medium will be a good example for testing how well our inversion works in nonidealized, realistic situations.

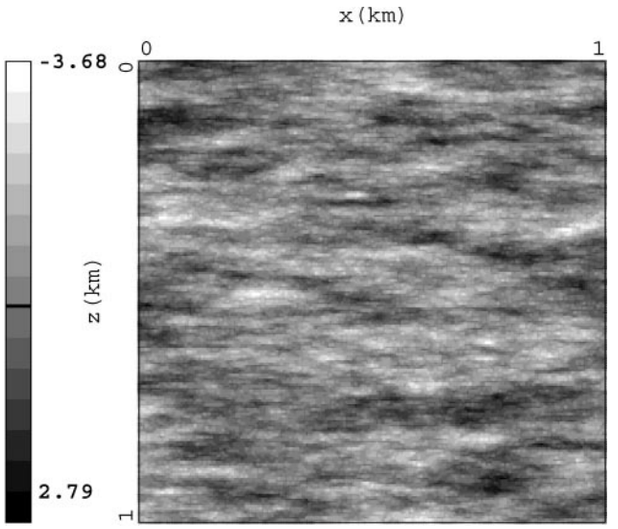

FIG. 1. One realization of a 2D anisotropic random perturbation with an exponential covariance, a variance $\sigma^2 = 1$, a horizontal correlation length $a = 0.1$ km, a vertical correlation length $b = 0.02$, which leads to an anisotropy ratio $\Lambda = a/b = 5$.

Wave propagation in random velocity model

We start with monochromatic waves, which obey the Helmholtz equation:

$$\Delta U + k^2 n^2 U = 0, \tag{4}$$

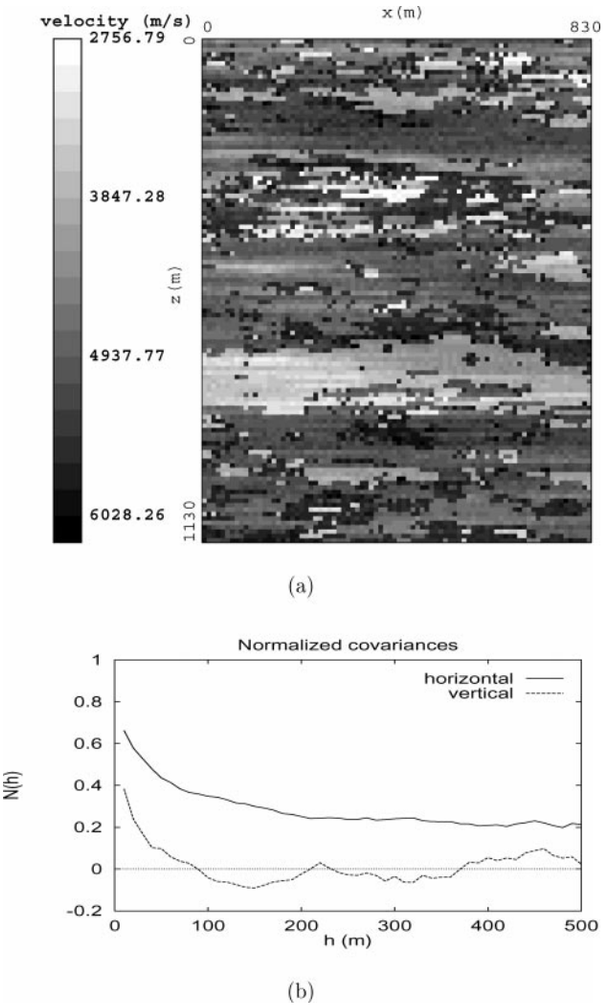

FIG. 2. (a) Seismic velocity model (in m/s) of the Texas reservoir. (b) Normalized velocity covariances in the horizontal and vertical directions of the velocity field of (a).

where U is the wavefield, k is the wavenumber, and n is the slowness field. We are studying the high-frequency regime $ka \gg 1$, $kb \gg 1$. Under these two conditions, scattered waves will for the most part propagate forward (small angles of diffraction). Moreover, we use the geometrical optics approximation where the wavefield U is written $U = Ae^{ikc_0T}$, with A and T the amplitude and traveltime of the wave. We will see later that the limitations induced by the geometrical optics are not very restrictive for our purpose; our inversion method gives acceptable results outside this regime.

In geometrical optics, the traveltime satisfies the eikonal equation:

$$[\nabla T(\mathbf{r})]^2 = n^2(\mathbf{r}). \tag{5}$$

We replace the slowness $n(\mathbf{r})$ by equation (1), where ϵ is a perturbation term. If $|\epsilon| \ll 1$, we can express T as a power series in ϵ: $T(\mathbf{r}) = T_0(\mathbf{r}) + T_1(\mathbf{r}) + O(\epsilon^2)$. We are looking for spherical wave solutions; keeping terms up to first order gives

$$T_0(\mathbf{r}) = \int_{\mathbf{r}} \frac{d\ell}{c_0\left(\frac{\ell}{r}\mathbf{r}\right)}, \tag{6}$$

$$T_1(\mathbf{r}) = \int_{\mathbf{r}} \frac{1}{c_0\left(\frac{\ell}{r}\mathbf{r}\right)} \epsilon\left(\frac{\ell}{r}\mathbf{r}\right) d\ell, \tag{7}$$

where $r = \|\mathbf{r}\|$ and the integration is performed along ray $\mathbf{r}$.

We suppose now that the variations of $c_0(\mathbf{r})$ along the ray are negligible. This is justified if the wave propagation length L is small compared to the model dimension because the macromodel $c_0(\mathbf{r})$ describes the very large velocity structure. Under this hypothesis, the integration path is straight at first order, and we obtain

$$T_0(\mathbf{r}) = \frac{r}{c_0(\mathbf{r})}, \tag{8}$$

$$T_1(\mathbf{r}) = \frac{1}{c_0(\mathbf{r})} \int_0^r \epsilon\left(\frac{\ell}{r}\mathbf{r}\right) d\ell. \tag{9}$$

Therefore, we obtain the traveltime covariance as

$$cov[T(\mathbf{r}_1), T(\mathbf{r}_2)] = \frac{1}{c_0(\mathbf{r}_1)c_0(\mathbf{r}_2)} \int_0^{r_1} \int_0^{r_2} \times \left\langle \epsilon\left(\frac{\ell_1}{r_1}\mathbf{r}_1\right) \epsilon\left(\frac{\ell_2}{r_2}\mathbf{r}_2\right) \right\rangle d\ell_1\, d\ell_2. \tag{10}$$

We see that if the macromodel is homogeneous ($c_0(\mathbf{r}) = c_0$), the covariance of the traveltimes can be calculated using the spatial covariance of the heterogeneities. This problem is explored in seismological literature [e.g., Wu and Flatté, (1990) for phases, Müller et al., (1992) for traveltimes]. Here, the measured traveltimes are the data. Our goal is thus to invert equation (10) properly to obtain estimates of the spatial distribution of the heterogeneities from the observed traveltime covariance.

To remove the effect of the macromodel, we divide the traveltime by its deterministic part (as in Klimeš, 2002b), and we call it the relative traveltime τ:

$$\tau(\mathbf{r}) = \frac{T(\mathbf{r})}{T_0(\mathbf{r})}, \tag{11}$$

$$cov[\tau(\mathbf{r}_1), \tau(\mathbf{r}_2)] = \frac{1}{r_1 r_2} \int_0^{r_1} \int_0^{r_2} \times \left\langle \epsilon\left(\frac{\ell_1}{r_1}\mathbf{r}_1\right) \epsilon\left(\frac{\ell_2}{r_2}\mathbf{r}_2\right) \right\rangle d\ell_1\, d\ell_2. \tag{12}$$

Inversion formula for spherical transmitted waves

We present here our algorithm for the transmission problem of spherical waves in the 2D case. Assume that we have measured all traveltimes $T(x, L)$, where x is the coordinate transverse to the wave propagation direction and L is the distance from the source to the receiver line (Figure 3). For example, in a crosswell seismic geometry, L would be the distance between the wells and x would be the distance along the receiver cable in the borehole. Our inversion algorithm has three parts: (1) retrieving the velocity covariance $C_\epsilon(r)$ and the correlation length transverse to the propagation direction; (2) retrieving the anisotropy ratio $\Lambda = a/b$ and then the correlation length parallel to the propagation direction; and (3) retrieving the variance of the velocity fluctuations σ_ϵ^2.

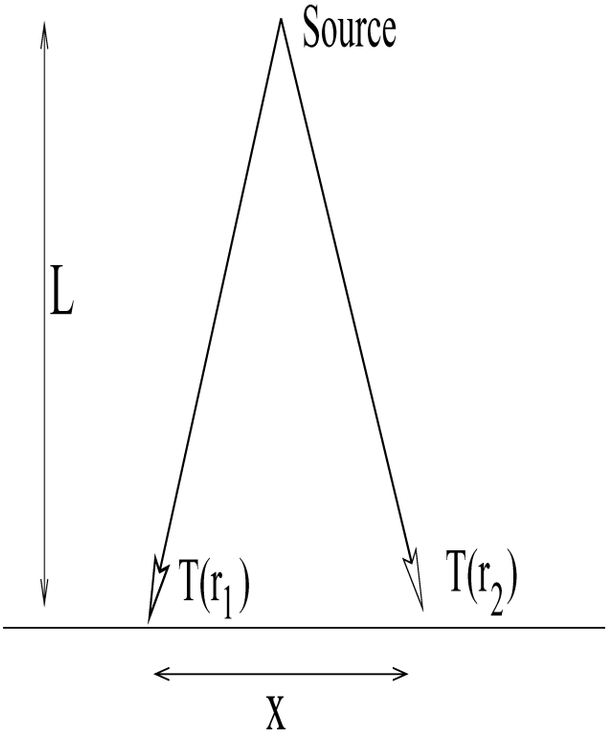

FIG. 3. Geometry of two straight rays leaving a point source. Traveltimes $T(\mathbf{r}_1)$ and $T(\mathbf{r}_2)$ are measured at a vertical distance L from the source and are laterally separated by a distance x.

Shape of the velocity covariance C_ϵ and transverse correlation length.—Let C_τ be $C_\tau(x, L) = cov[\tau(x_1, L), \tau(x_2, L)]$ with $x = |x_1 - x_2|$. In the case of a near-vertical propagation direction and provided the offset is small ($x \ll L$), equation (12) gives (Chernov, 1960; Rytov et al., 1987)

$$C_\tau(x, L) = \frac{2}{xL}\sigma_\epsilon^2 \int_0^x \int_0^{+\infty} N(u, z)\, du\, dz. \tag{13}$$

This is the Chernov approximation, valid only if the wave has crossed many heterogeneities during its propagation, i.e, $b \ll L$ (b is the characteristic vertical size of heterogeneities). For instance, when $N(u, z) = \exp[-((u^2/a^2) + (z^2/b^2))]$ (Gaussian covariance), equation (13) can be written $C_\tau(x, L) = (2\sqrt{\pi}\sigma_\epsilon^2/xL)\{b/2 + a[g(\sqrt{2}x/b) - 1/2]\}$ where $g(t) = (1/\sqrt{2\pi}) \int_{-\infty}^{t} e^{-z^2/2}\, dz$ is the normal distribution function.

Let the function $I(x)$ be

$$I(x) = \frac{\partial}{\partial x}[xC_\tau(x, L)]. \tag{14}$$

In Appendix A, we derive the inversion formula from equation (13):

$$C_\epsilon\left(\frac{r}{a}\right) = \frac{\left[\displaystyle\int_r^{+\infty} \frac{\dfrac{\partial I(x)}{\partial x}}{\sqrt{x^2 - r^2}}\, dx\right]}{\left[\displaystyle\int_0^{+\infty} \frac{\dfrac{\partial I(x)}{\partial x}}{x}\, dx\right]}. \tag{15}$$

This is the formula to calculate the velocity covariance from the relative traveltime covariance. For estimating the correlation length a, the algorithm is slightly different, depending on the type of covariance model. The method is to plot the right-hand side of equation (15) as a function of r, and a is obtained as the abscissa of the curve point whose ordinate is $C_\epsilon(r/a)|_{r=a} = C_\epsilon(1)$. If the shape of C_ϵ is Gaussian or exponential, then $C_\epsilon(1) = e^{-1}$.

Remark 1: If the macromodel is homogeneous, we can obtain C_ϵ directly from the traveltimes $T(x, L)$ with formula (15) and $I(x) = (\partial/\partial x)[xC_T(x, L)]$. Moreover, for plane waves propagating from $z = 0$ to $z = L$, the inversion formula is the same with $C_T(x, L) = cov[T(x_1, L), T(x_2, L)]$ replacing $I(x)$ in equation (15) (Iooss, 1998b).

Remark 2: in 3D statistically TI media, inversion formulas (14), (A-4), and (15) are the same (Iooss, 1998b), with $C_\tau(x, L) = cov[\tau(x_1, y_1, L), \tau(x_2, y_2, L)]$, where $x = \sqrt{(x_1 - x_2)^2 + (y_1 - y_2)^2}$.

The anisotropy ratio Λ.—From equation (12) we get (Chernov, 1960; Samuelides and Mukerji, 1998)

$$var[\tau(0, L)] = \frac{2\sigma_\epsilon^2}{L} b \int_0^{+\infty} C_\epsilon(r)\, dr, \tag{16}$$

$$var[\tau(L, L)] = \frac{2\sigma_\epsilon^2}{L} \frac{2}{\sqrt{\dfrac{1}{a^2} + \dfrac{1}{b^2}}} \int_0^{+\infty} C_\epsilon(r)\, dr. \tag{17}$$

Therefore, we have

$$\zeta = \frac{var[\tau(L, L)]}{var[\tau(0, L)]} = \frac{2\Lambda}{\sqrt{1 + \Lambda^2}}, \tag{18}$$

which gives $\Lambda = \zeta/\sqrt{4 - \zeta^2}$. The anisotropy ratio Λ can thus be deduced from the normalized variance $var[\tau(L, L)]/var[\tau(0, L)]$. The right-hand side of equation (18) does not depend on the type of covariance, only on the anisotropy ratio. Therefore, the numerical error made in the estimation of C_ϵ in the first stage does not influence the estimation of Λ.

Equation (18) can be replaced by the more general formula (Iooss, 1998b)

$$\zeta = \frac{var[\tau(x, L)]}{var[\tau(0, L)]} = \frac{\Lambda}{\cos(\alpha)\sqrt{\sin^2(\alpha) + \Lambda^2 \cos^2(\alpha)}}, \tag{19}$$

where $\sin(\alpha) = x/\sqrt{x^2 + L^2}$. However, x must be greater than or comparable to L to get an accurate estimate of Λ. This requirement on the offset x is not consistent with the offsets used in the first stage, where we required $x \ll L$. Furthermore, ζ is not very sensitive to Λ. In Figure 4 we plot ζ as a function of Λ for different x/L ratios. As we can see, the curves flatten out quickly and are not very sensitive to the anisotropy ratio.

This means that the anisotropy ratio method is not applicable for acquiring the geometry of Figure 3. However, the anisotropy ratio can be estimated by considering traveltimes of waves propagating along two quasiperpendicular directions (Iooss and Samuelides, 1998). For example, in a real data case we can consider crosswell and VSP experiments.

The variance of velocity fluctuations σ_ϵ^2.—At this stage, we know the values of L (propagation distance), a and b (horizontal and vertical correlation lengths), and of the standardized covariance C_ϵ. Then we can get the variance of fluctuations σ_ϵ^2 from equation (16).

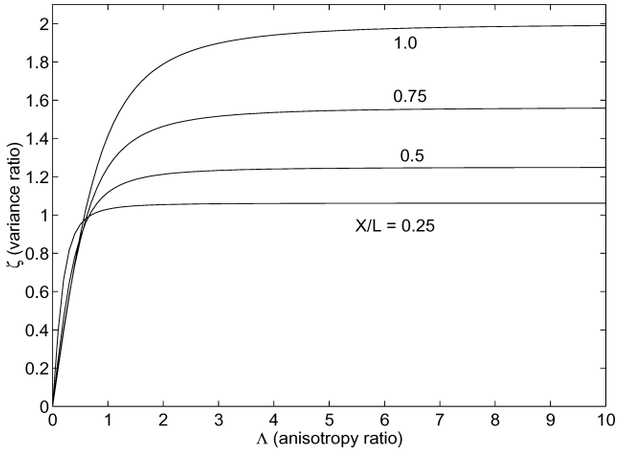

FIG. 4. Traveltime variances ratio $\zeta = varT(X, L)/varT(0, L)$ as a function of Λ [equation (19)], for different values of X/L.

Recall of validity domains

In this section, we detail the validity domains of the previous theory. Let us call $\ell_\parallel$ and $\ell_\perp$ the correlation lengths parallel and transverse to the propagation direction. For near-vertical propagation, which is the case of seismic reflection data, we must use the horizontal parameter $\ell_\perp = a$ and the vertical one, $\ell_\parallel = b$.

First, use of random media requires $\ell_\parallel \ll L$, with L the wave propagation distance (the wave must meet many heterogeneities during its propagation). Moreover, the separation between macromodel and midscale model needs the hypothesis that $L \ll$ domain dimension (no variations of the macromodel during propagation). To simplify the covariance formula (Chernov approximation), we also suppose that $x \ll L$, i.e., the lateral separation between receivers is much smaller than the propagation distance.

In the theoretical part, we use a first-order perturbation solution of the eikonal equation (5). Iooss et al. (2000) derive the validity domain of the traveltime variance computation:

$$L \ll K\left(\frac{\ell_\perp^4}{\ell_\parallel}\right)^{1/3}\sigma_\epsilon^{-2/3}, \tag{20}$$

where σ_ϵ is the standard deviation of velocity perturbation and K is a constant depending only on the covariance structure. The validity domain increases with $\ell_\perp$ and decreases with $\ell_\parallel$. Indeed, in this case rays deviate more easily from straight-line propagation.

In addition to the high-frequency hypothesis ($k\ell_\parallel \gg 1$ and $k\ell_\perp \gg 1$ with k the wavenumber), we use geometrical optics to perform our derivations. Strictly speaking, the geometrical optics theory is only valid when diffraction effects can be neglected. This condition may be written as (Samuelides and Mukerji, 1998)

$$D = \frac{4L}{k\ell_\perp^2} \ll 1, \tag{21}$$

where D is the wave parameter. If condition (21) is not fulfilled, a relation still exists between the covariance of the media and the covariance of the traveltimes. It can be investigated by using the Rytov approximation instead of the geometrical optics approximation (Iooss, 1998a; Samuelides, 1998).

It turns out that the formula given by geometrical optics overestimates the traveltime covariance obtained from the Rytov approximation by a factor γ ($1 \le \gamma \le 2$), which is an increasing function of D, with two being its maximum value (Rytov et al., 1987; Iooss, 1998a). This has a very small effect on the first two parts of our algorithm [equations (15) and (18)] because we deal with ratios of covariances (or variances) and the factor γ of the numerator is very close to that of the denominator. However, this overestimation can have an effect on the estimate of the variance of the velocity fluctuations [equation (16)]: if $D > 1$ (geometrical optics not applicable), our algorithm would underestimate σ_ϵ^2 by the factor of γ (at most two). Therefore, a need to estimate σ_ϵ^2 accurately with large distances of propagation could motivate the elaboration of an inversion method based on the Rytov approximation.

STATISTICAL TOMOGRAPHY FOR SEISMIC REFLECTION DATA

In exploration seismic techniques, the available information is most commonly in the form of reflection traveltimes. We present two methods of inversion of the velocity covariance C_ϵ: one using prestack data (prestack statistical tomography), and one more robust but less precise using the stacking velocities (poststack statistical tomography).

Inversion of prestack traveltimes

To find correlations of traveltimes reflected by an interface, we decompose the travelpath $\mathbf{r}$ (from source to receiver) into a downgoing part $\mathbf{r}_1$ and an upgoing part $\mathbf{r}_2$. To characterize statistics of the velocity field, it is sufficient to work with the variance of traveltimes $T(x)$ at constant offset x (source–receiver distance). As $T(x) = T(\mathbf{r}) = T(\mathbf{r}_1) + T(\mathbf{r}_2)$, we obtain

$$var[T(x)] = var[T(\mathbf{r}_1)] + var[T(\mathbf{r}_2)] + 2cov[T(\mathbf{r}_1), T(\mathbf{r}_2)]. \tag{22}$$

Here we want to work with the relative traveltime $\tau(\mathbf{r}) = T(\mathbf{r})/T_0(\mathbf{r})$. Therefore, we have to suppose that downgoing and upgoing macromodel traveltimes are equal: $T_0(\mathbf{r}_1) = T_0(\mathbf{r}_2) = T_0(\mathbf{r})/2$. This is acceptable if $c_0(\mathbf{r})$ varies neither vertically nor on a lateral distance of x. Then

$$\begin{aligned} var[\tau(x)] &= var\left[\frac{T(\mathbf{r}_1)}{2T_0(\mathbf{r}_1)} + \frac{T(\mathbf{r}_2)}{2T_0(\mathbf{r}_2)}\right] \\ &= var\left[\frac{\tau(\mathbf{r}_1)}{2}\right] + var\left[\frac{\tau(\mathbf{r}_2)}{2}\right] \\ &\quad + 2cov\left[\frac{\tau(\mathbf{r}_1)}{2}, \frac{\tau(\mathbf{r}_2)}{2}\right]. \end{aligned} \tag{23}$$

For a horizontal reflector located at a depth $z = L_0$, we find up to first order (Touati, 1996; Touati et al., 1999)

$$var[\tau(x)] = \frac{1}{2}[C_\tau(0, L_0) + C_\tau(x, L_0)], \tag{24}$$

where $C_\tau(0, L_0)$ is defined by equation (13) and $C_\tau(0, L_0) = var[\tau(0, L_0)$ is defined by equation (16). This expression is valid for all offsets $x < L_0$.

The value $var[\tau(x)]$ depends on the reflector depth L_0, on the offset x, and on the covariance $N(\mathbf{r})$, which is described by the statistical parameters C_ϵ, σ_ϵ, a, and b. The normalized relative traveltime variance $var[\tau(x)]/var[\tau(0)]$ does not depend on L_0, on c_0, on the perturbation variance σ_ϵ^2, and on the vertical correlation length b. Therefore, a fitting procedure of $var[\tau(x)]/var[\tau(0)]$ can be derived to retrieve the standardized covariance C_ϵ and the horizontal correlation length a (Touati, 1996; Iooss, 1998a).

As for transmitted waves [equations (14) and (15)], we also derive the direct inversion of C_ϵ:

$$I_R(x) = \frac{\partial^2}{\partial x^2}\{x\,var[\tau(x)]\} = \frac{\partial^2}{2\partial x^2}[xC_\tau(x, L_0)], \tag{25}$$

$$C_\epsilon\left(\frac{x}{a}\right) = \frac{\left[\displaystyle\int_x^\infty \frac{I_R(x')}{\sqrt{x'^2 - x^2}}\,dx'\right]}{\left[\displaystyle\int_0^\infty \frac{I_R(x')}{x'}\,dx'\right]}. \tag{26}$$

Reflector fluctuations

If the reflector has a large-scale irregularity (smooth variations on a kilometric scale), $var[\tau(x)]$ depends on the relative

point of reflection depths of each traveltime. We note the relative traveltime $\tau_{\mathbf{m}}(x)$ (where $\mathbf{m}$ is the midpoint between source and receiver) which is no longer stationary. Then we cannot work with its variance. The problem is to remove the reflector geometry dependence of $\tau_{\mathbf{m}}(x)$. Practically, this can be done using a curve fitting of $\tau_{\mathbf{m}}(x)$. For example, we can compute a polynomial regression for each x using least squares. Thus, the residual relative traveltimes $\tau'(x)$ are stationary, and their variance corresponds to the traveltime variance in the same medium with a horizontal reflector (Iooss, 1998b).

A more difficult problem is the fine-scale fluctuations of the reflector (variation on a hectometric scale). From traveltimes, deterministic techniques cannot filter the fluctuating part because of the reflector perturbations, and the fluctuating part because of the velocity heterogeneities. To study this problem for the statistical tomography process, we introduce a stochastic model of the interface:

$$L(x) = L_0 + \eta(x), \tag{27}$$

where $L(x)$ is the reflector depth, L_0 is the constant average depth, and η is a stationary centered random function ($\langle\eta\rangle = 0$), with covariance $C_\eta(x)$, standard deviation σ_η, and correlation length l_η. The values σ_η and ℓ_η are the typical value and length of the fluctuations; η is assumed to be smooth, with weak and slow variations, such that the waves only reflect and do not diffract on the interface. Mathematically, these hypotheses can be written as (Iooss, 1998b)

$$\sqrt{\lambda\sigma_\eta} \ll \frac{\ell_\eta}{2}, \quad \sigma_\eta \ll L_0 \quad \text{and} \quad \sigma_\eta \ll \ell_\eta. \tag{28}$$

Studying the traveltimes $T_0(x)$ in a homogeneous velocity field c_0 for a random reflector respecting equation (28) and for small offsets ($x < L_0$), Iooss (1998b) shows that the traveltime variance at first order is constant in function of the offset and can be expressed as

$$var[T_0(x)] = \frac{4}{c_0^2}\sigma_\eta^2. \tag{29}$$

For the relative traveltimes $\tau_0 = T_0/T_0^0$ (where $T_0^0(x)$ is the traveltime for constant velocity and horizontal planar reflector), we obtain up to first order

$$var[\tau_0(x)] = \frac{\sigma_\eta^2}{L_0^2}. \tag{30}$$

Using first-order geometrical optics, it is possible to link the stochastic velocity and reflector models (Iooss and Galli, 2000). The traveltime variance for random velocity and reflector consists of two terms—one with a constant depth L_0 and a random velocity, one with a constant velocity c_0 and a random depth:

$$var[\tau(x)] = \frac{1}{2}\left[C_\tau(0, L_0) + C_\tau(x, L_0) + \frac{\sigma_\eta^2}{L_0^2}\right]. \tag{31}$$

One very interesting result as a consequence of formula (31) is that the direct inversion of the velocity covariance with equation (26) remains valid. Indeed, $I_R(x)$ is unchanged because the additional term σ_η^2/L_0^2 in $var[\tau(x)]$ is constant, Then

$$I_R(x) = \frac{\partial^2}{\partial x^2}\{x\, var[\tau(x)]\} = \frac{\partial^2}{2\partial x^2}[2xC_\tau(x, L_0)]\ . \tag{32}$$

Robust inversion in terms of stacking velocity

Geraets and Galli (2002) express the covariance between the stacking velocities as a function of the covariance of the perturbations of the instantaneous velocity field. If we denote $T_{\alpha i}$ as the traveltime for a wave generated by the source, reflecting on the CMP α of the horizontal interface and arriving on the ith receiver, we show in Appendix B that the covariance of the stacking velocities $V_{st\alpha}$ and $V_{st\beta}$ for two CMPs α and β can be expressed as

$$cov(V_{st\alpha}, V_{st\beta}) \simeq \frac{c_0^6}{4}\sum_{i=1}^{n}\sum_{j=1}^{n} k(i, j, n)\, cov\left(T_{\alpha i}^2, T_{\beta j}^2\right), \tag{33}$$

with

$$cov\left(T_{\alpha i}^2, T_{\beta j}^2\right) \simeq 4\langle T_{\alpha i}\rangle\langle T_{\beta j}\rangle cov(T_{\alpha i}, T_{\beta j}) + cov(T_{\alpha i}, T_{\beta j})^2 - var(T_{\alpha i})var(T_{\beta j}). \tag{34}$$

The value $cov(T_{\alpha i}, T_{\alpha j})$ is the covariance between two reflection traveltimes (given in Appendix C). The term $k(i, j, n)$ is a function of the layout:

$$k(i, j, n) = \frac{n^2x_i^2x_j^2 - nx_j^2\left(\sum_{\ell=1}^{n} x_\ell^2\right) - nx_i^2\left(\sum_{\ell=1}^{n} x_\ell^2\right) + \left(\sum_{\ell=1}^{n} x_\ell^2\right)\left(\sum_{\ell=1}^{n} x_\ell^2\right)}{\left[n\sum_{\ell=1}^{n} x_\ell^4 - \left(\sum_{\ell=1}^{n} x_\ell^2\right)\left(\sum_{\ell=1}^{n} x_\ell^2\right)\right]^2}, \tag{35}$$

with x_i the offset of the ith receiver and n the number of receivers used for the velocity analysis. Once the acquisition parameters are defined, expression (33) provides the theoretical covariance of the stacking velocities for any given model of the instantaneous velocity field.

Using this expression in an iterative procedure to fit the experimental results (the covariance curve obtained for stacking velocity profiles), we obtain a good estimate of the horizontal correlation length of the velocity perturbations. Tests (not presented here) have shown that the fitting must concentrate on the location of the first minimum of the experimental covariance curve.

Note in this expression the joint impact of the covariance function of the velocity perturbations and of the acquisition layout. An increase of the size of the acquisition layout (using more geophones or increasing the distance between them) increases the first minimum position of the theoretical correlation curve, as does an increase of the

horizontal correlation length of the velocity perturbation field.

SYNTHETIC TESTS OF STATISTICAL TOMOGRAPHY

With seismic reflection experiments, previous works describe the inversion of the horizontal correlation length for a constant velocity background. Touati et al. (1999), Iooss (1998a), and Geraets and Galli (2002) use horizontal reflectors, while deterministic or random reflector fluctuations are considered by Iooss (1998b) and Iooss and Galli (2000). These works also make some parametric studies of the statistical tomography resolution in terms of the velocity correlation lengths. In summary, they show we can retrieve correlation lengths larger than twice the dominant wavelength. Moreover, the estimation error is at most 20%, even if the geometrical optics approximation does not hold (Iooss, 1998a).

The goal of the following tests is to illustrate the inversion methods by keeping our basic hypothesis of geometrical optics. Therefore, to simulate synthetic data, we use algorithms such as ray tracing and eikonal solvers. We compare prestack and poststack statistical tomography in an idealized velocity field. We then apply the direct inversion of the velocity covariance (prestack statistical tomography) in media with macroscale lateral variations. Finally, we test, using transmission data, the direct inversion approach in a realistic complex medium, violating the stationarity and geometrical anisotropy hypotheses [equations (2) and (3)].

Seismic reflection in idealized medium

We test the two statistical tomography algorithms for seismic reflection geometry, limiting the propagation in one layer containing a single seismic reflector. The total field of each model covers 20×1 km. Interface and velocity models are parameterized by cubic B-spline functions (Inoue, 1986). We compute 182 synthetic shot records (with a 0.1-km spacing) using a ray-tracing algorithm based on the bending technique (Jurado et al., 1998). The first source is placed at 0.2 km from the left corner, and all of the sources and receivers are at the surface ($z = 0$). Each shot record consists of 16 traveltimes T with offset ranging from 0 to 1.5 km with a 0.1-km spacing. White noise with a 1-ms standard deviation is superimposed on the calculated traveltimes to simulate the plausible random error that we have when we pick traveltimes from seismic traces (from time sampling). However, on real data, picking noise is much more complex.

The scenario is very simple, respecting the basic application conditions: horizontal reflector (depth $L_0 = 0.95$ km) and constant background velocity (Figure 5a). The mean of the velocity field is 2 km/s. The small velocity fluctuations ($\sigma_\epsilon = 4\%$) have a Gaussian covariance and heterogeneity scales ($a = 0.4$ km, $b = 0.1$ km). The random media are simulated using the turning bands technique (Matheron, 1973; Lantuéjoul, 1994).

To invert the traveltimes for the velocity macromodel, we use the reflection tomography software of Jurado et al. (1998). We minimize the cost function $C(m) = \sum_{i=1}^{N} (T_i^{cal} - T_i^{obs})^2/\sigma_i^2 + R$, where m is the earth model (velocity and reflector), N is the number of dataprints, T^{obs} are the observed traveltimes, T^{cal} are the calculated traveltimes, σ_i is the standard deviation of the uncertainty associated with data T_i^{obs}, and R is a regularization term. A priori information is introduced in R by regularization weights on the second derivatives of the model (Delprat-Jannaud and Lailly, 1993). Our goal is to retrieve a very smooth macromodel m, so we keep strong regularization weights. The result of tomography is shown in Figure 5b. The inverted velocity macromodel is homogeneous, and the inverted reflector is horizontal with a perfectly reproduced depth ($L_0 = 0.95$ km).

First, we apply prestack statistical tomography on the relative traveltimes: we calculate the traveltimes T_0 in the inverted medium and we obtain the relative traveltimes $\tau = T/T_0$. To have a smooth curve for robust differentiation and integration, we do a least-squares fourth-order polynomial fit to the experimental traveltime variance versus constant offset curve. Then we apply the Abel transform on the normalized polynomial and obtain the standardized velocity covariance by equation (26).

For the integration and the polynomial fit, we compare the results of using all of the relative traveltime variance curve or

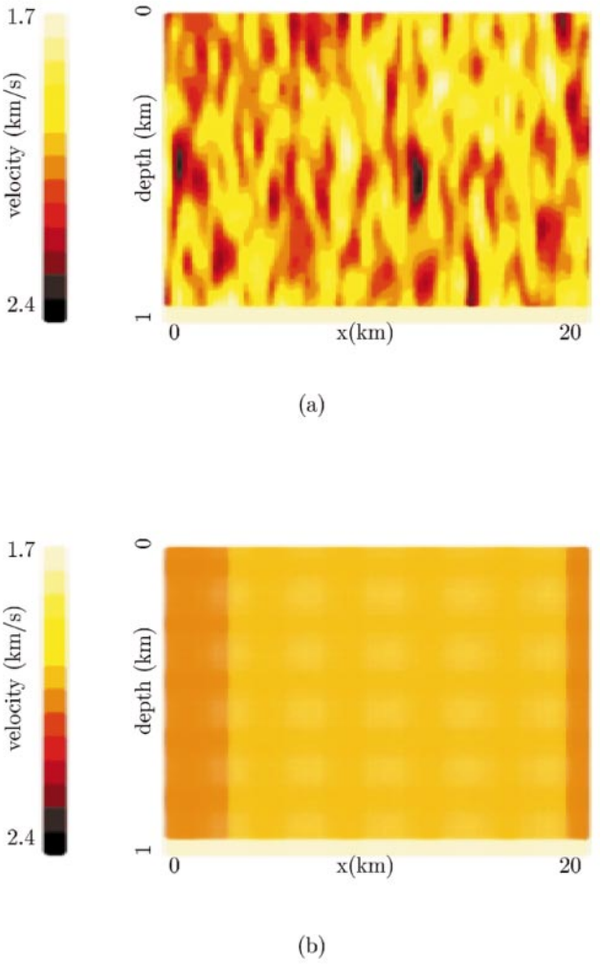

FIG. 5. (a) True synthetic velocity model (Gaussian covariance, $\sigma_\epsilon = 4\%$, $a = 0.4$ km, $b = 0.1$ km, $\Lambda = 4$) with horizontal reflector. (b) Inverted velocity model by traveltime tomography.

only the initial part with a cutoff at $x = L_0$ (Figure 6a). Indeed, the behavior of the initial part of the variance–offset curve, as its slope decreases to zero, is important. Moreover, errors increase with large lag values, and the experimental traveltime variance is no longer reliable. In the two cases, the shape of the inverted velocity covariances is well retrieved compared to the true Gaussian covariance (Figure 6b). For the estimate of the correlation length a (the true value is 0.4 km), we take the abscissa corresponding to e^{-1}, and we obtain 0.46 km (15% error) with the cutoff curve and 0.5 km with the full curve. The choice of the cutoff $x = L_0$ is justified by the fact that formula (24) is valid for $x < L_0$.

Second, we apply poststack statistical tomography on the same data. Stacking velocity analysis is performed, using a hyperbolic fit of the traveltimes CDP gathers. On Figure 7a we show the stacking velocity profile obtained. Although the velocity fluctuations have very reduced amplitude ($\sigma_\epsilon = 4\%$), the stacking velocity estimations vary from 1830 to 2230. The covariance of the stacking velocity profile is given in Figure 7b, with the proposed theoretical curve computed using equation (33). This satisfying fit is found after a few attempts. It corresponds to an estimate of 0.32 km (20% error) for the horizontal correlation length of the velocity fluctuations. Because of the stacking process and the evaluation of complex integral formulas, the poststack statistical tomography is expected to be less precise in synthetic cases than the prestack method. This is true with a reduced data set, but in the present case we see that the size of the seismic line allows us to obtain an estimate of the correlation length almost with the same precision using this alternative method.

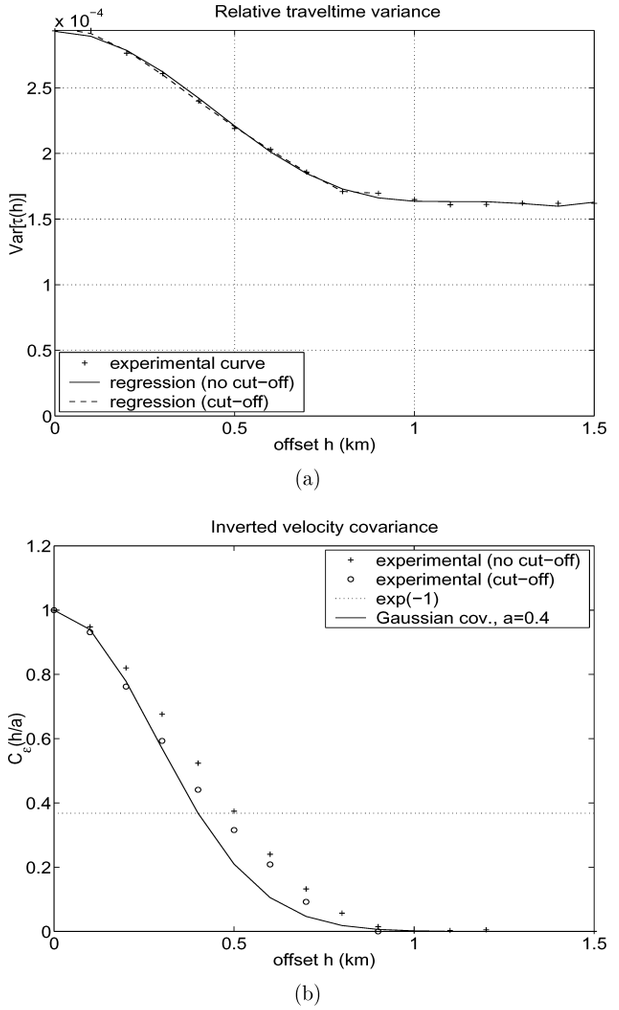

FIG. 6. (a) Experimental relative traveltime variance as a function of the offset (calculated from synthetic traveltimes and after tomography) corresponding to the model in Figure 5a. The two polynomial fits are calculated by least-squares regression. (b) Inverted velocity covariances by prestack statistical tomography for the two different fits. Comparisons are made with the true velocity covariance (Gaussian curve).

Seismic reflection in idealized medium with macroscale variations

We apply the prestack statistical tomography process to a more complex scenario with random fluctuations and deterministic variations of reflector and velocity. The geometric and acquisition parameters are the same as in the previous case,

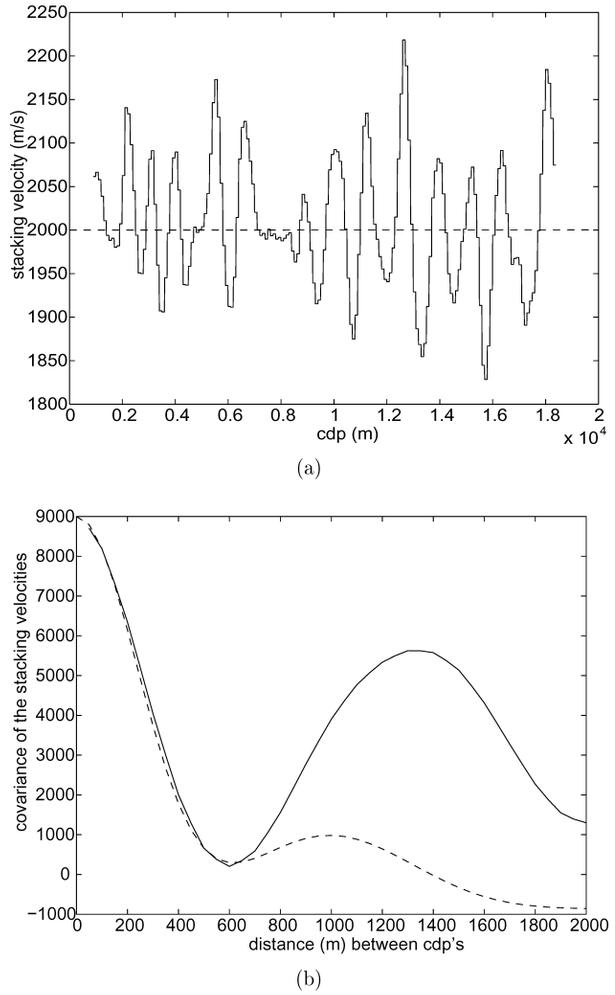

FIG. 7. (a) Results of the velocity analysis process corresponding to the model in Figure 5a. (b) Stacking velocity covariances in $(m/s)^2$ (full curve) and its fit (dotted curve).

and we follow exactly the same inversion process as before. In this case, the poststack approach is not considered because of the violation of all the hypotheses of the stacking velocity analysis.

Figure 8a shows the medium, which has a syncline structure in terms of reflector (a gradient of 0.02 km^{-1} followed by a gradient of -0.02 km^{-1}) and velocity (a horizontal gradient of -0.05 s/km followed by a horizontal gradient of 0.05 s/km). The random velocity fluctuations are the same as in the previous test. Moreover, the reflector has random fluctuations ($\sigma_\eta/L_0 = 1\%$) with a Gaussian covariance and a correlation length of $\ell_\eta = 0.4$ km. The result of tomography is shown in Figure 8b. We obtain a good representation of the large velocity variations, while the reflector trend is respected with small departures. The relative traveltime variance (Figure 9a) shows a smaller decrease than in the previous case (Figure 6a). This is from the additive term corresponding to random reflector fluctuations [equation (31)]. For the velocity covariance inversion (Figure 9b), we obtain a good estimate of the Gaussian covariance and the horizontal correlation length: 0.37 km compared to the true value of 0.4 km (7.5% error).

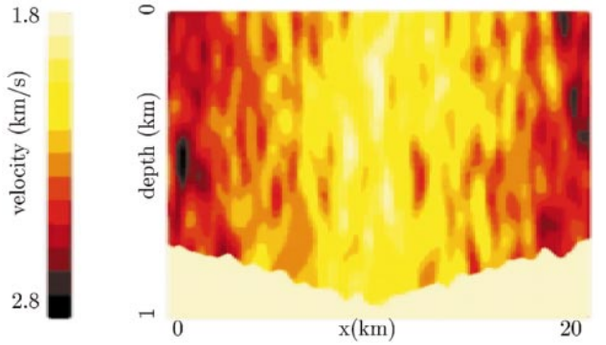

(a)

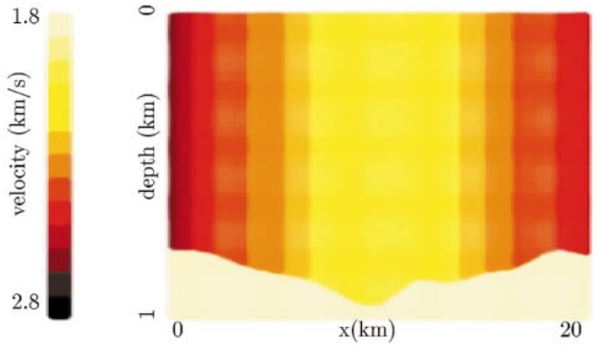

(b)

FIG. 8. (a) True synthetic velocity model (horizontal gradient, Gaussian covariance, $\sigma_\epsilon = 4\%$, $a = 0.4$ km, $b = 0.1$ km, $\Lambda = 4$) and reflector (gradient, Gaussian covariance fluctuations, $\ell_\eta = 0.4$ km). (b) Inverted velocity model by traveltime tomography.

This is a very satisfactory result because it shows that the prestack statistical tomography formulation works even in the case of large reflector variations (not modeled by the theory). However, we believe that this result is better than the result of the previous simpler example because of compensatory errors induced by the large reflector trend. This induced some bias in our inversion algorithm, which decreases the estimate of the correlation length. We can conclude that we have applied succesfully, and for the first time, the statistical tomography process to a velocity model containing lateral deterministic trend with small gradients. Velocity fields with complex structures are certainly outside the scope of our methods.

Seismic transmission in realistic medium

We test the prestack statistical tomography process for transmission data in a realistic synthetic medium shown in Figure 2a. The method of numerical propagation is a finite-difference

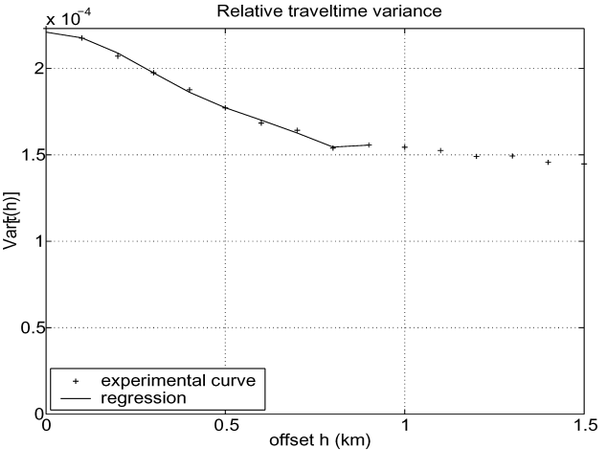

(a)

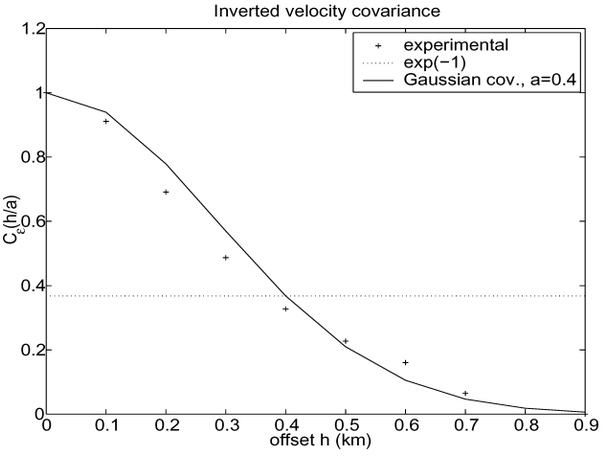

(b)

FIG. 9. (a) Experimental relative traveltime variance as a function of the offset corresponding to the model in Figure 8a. The polynomial fit is calculated by least-squares regression. (b) Inverted velocity covariance by prestack statistical tomography. Comparison is made with the true velocity covariance (Gaussian curve).

code based on the eikonal equation (Podvin and Lecomte, 1991). This method requires little CPU time, directly gives the arrival times, and considers both transmitted and diffracted rays.

First, we propagate a traveling plane wave along the horizontal direction. A line source is placed at the left edge of the model ($x = 10$ m). The traveltimes are calculated along one vertical line of receivers at a sufficiently large propagation distance $L = 800$ m. Ninety receivers have a vertical spacing of $dz = 10$ m, with the topmost receiver at $z = 120$ m. In the second geometry, a plane-wave is propagated along the vertical direction. The plane wave source is placed at the top edge of the model ($z = 10$ m). The traveltimes are also calculated along one horizontal line of receivers at the propagation distance $L = 800$ m. Sixty receivers are spaced at $dx = 10$ m with the first receiver at $x = 120$ m.

In this test, we assume that the macromodel is homogeneous; we directly use the normalized covariance of the vertical (respectively, horizontal) traveltimes to estimate the horizontal (vertical) statistical structure. We look at the normalized traveltime covariances in Figure 10a. We invert C_ϵ from the normalized traveltime covariance [equation (15) and Remark 1]. The polynomial fit is similar to the one described previously. For the vertical wave, the decrease of the traveltime covariance is slow, and 21 points can be used. The inversion (Figure 10b) gives a velocity horizontal covariance with a range of $A = 195$ m. For the horizontal wave, the decrease is fast and only nine points could be used. On the inverted velocity covariance (Figure 10b), we can fit a covariance model with $B = 75$ m.

Large discrepancies appear on the shape of the inverted covariances. First, the horizontal covariance converges to zero, while the initial horizontal covariance converges to 0.24. This is from the zonal anisotropy (instead of geometrical anisotropy). Moreover, because of the nugget effect, the decrease of the initial velocity covariances is much stronger than the inverted covariance. The nugget effect is a very localized phenomenon that can only be measured by the variance of the interest variable. Therefore, by propagating waves in this model, we cannot measure such small-scale local structures. Because of the nugget effect and the nonstationarity, the experimental covariance shapes do not fit the initial model curves. However, ranges are well estimated: $B = 75$ m versus true value of 65 m and $A = 195$ m versus true value of 160 m. The errors are of the order of 20%.

The model in this case does not fully respect the assumptions of the theory because the velocity covariance is not of the types of equations (2) and (3). In addition, for a horizontally traveling plane wave, condition (20) does not seem to be satisfied. We approximately evaluate $K\sigma_\epsilon^{-2/3}(B^4/A)^{1/3} = 278$ m by taking $K = 1.65$ (value of the Gaussian covariance case), and we see that $L = 800$ m is larger than 278. However, the range estimates from the inversion are reasonably good. This suggests that the algorithm could be useful in actual nonidealized field situations.

APPLICATION TO REAL DATA

We now apply the two algorithms (prestack and poststack statistical tomography) to a real data set, provided by Eni-Agip division. We receive four parallel seismic lines (A, B, C, and D) from a 2D marine acquisition, having undergone a minor pre-processing (edition, mute). Figure 11a shows a near-offset seismic section of one line. The acquisition layout is comprised of 46 hydrophones, 50 m apart. The distance between shot points is 50 m. One single reflector (marked with white arrows in Figures 11a and 11b) is picked in prestack domain between the two-way traveltimes 3.7 s (at left corner) and 3.5 s (at right corner). This reflector is almost horizontal, in accordance with our general hypothesis. The vertical correlation length of the velocity field is derived from the sonic logs available in the area: we obtain an estimated value of 80 m.

Using prestack picking, we can study the behavior of the common-offset collections of arrival times and model their variance as a function of the offset. For two of our lines, the resulting curve does not present the expected behavior: the variance of the picked times increases with offset. Such a behavior may result from different kinds of problems: it is possible that the hypothesis of local stationarity of the reflector is no longer

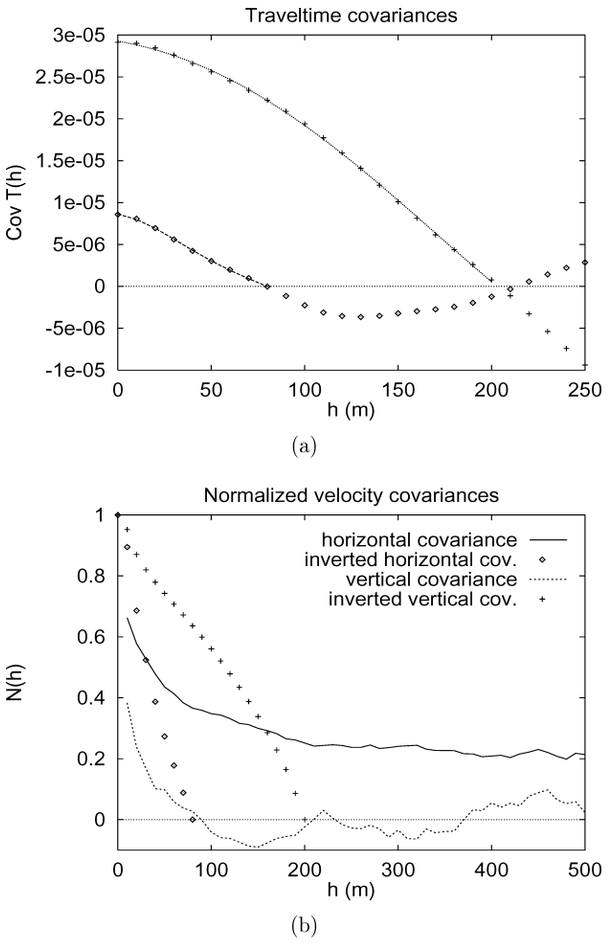

FIG. 10. Results on the Texas model (Figure 2a). (a) Traveltime covariances; as a function of the offset (crosses: vertical covariance, diamonds: horizontal covariance) and their polynomial fits by least-squares regression. (b) True normalized velocity covariances (in the horizontal and vertical directions) and the inverted curves from covariances of synthetic traveltimes.

valid in the considered area, in which case the variance resulting from the local drift of the times can totally hide the offset dependence of the variance that we want to model. Another explanation comes from the prestack picking: as it works using a greedy algorithm, it first extends along the shot line and then starts growing in the direction of the bigger offsets. Also, the lower frequency of the far-offset records does not give access to a signal recognition as precise as with the small-offset records. Other explanations have been considered, but we finally decided to disregard these two lines when estimating the horizontal correlation length.

The normalized variance curves obtained for the two remaining lines show the general behavior predicted by the prestack statistical tomography. These curves are shown on Figure 12, together with the theoretical curve obtained using a Gaussian covariance and a horizontal correlation length of 1200 m.

To compare this result with the poststack statistical tomography, we apply the method using the stacking velocity profiles on the same data set. Figure 13a shows the four experimental covariances of the stacking velocity profiles. In Figure 13b, we see how the mean experimental covariance can be fitted using a Gaussian covariance model for the perturbations of the instantaneous velocity field with a horizontal correlation length of 800 m.

The estimations obtained using both methods are roughly similar and give a mean value of 1 km for the horizontal correlation length. Unfortunately, we cannot check this value because very few wells are available in this area. The second method seems to be more robust than the first one because it is less sensitive to the low quality of our data set (the prestack picking is not perfectly stable as a result of the important noise observed in some CDP gathers). It also has the advantage of requiring only the knowledge of the stacking velocities, instead of a complete prestack picking of the data set. This makes it easier to put into practice in an industrial context. On the other hand, if traveltime picking is correct, this method gives less precise estimates than the first method because of more complex formulas and because of the imprecision of the stacking velocity analysis. We leave to further study the differences between the two methods (in our tests estimates are smaller with the poststack method than with the prestack one).

CONCLUSIONS

We have presented two approachs for inverting the second-order statistics of the observed traveltimes to estimate the spatial covariance of the heterogeneous velocity field. Equations (15), (19), (26), and (33) constitute the main formulas of this paper. For the first method, prestack statistical tomography, we extend the work of Touati (1996) and Iooss (1998b) to a velocity macromodel containing lateral variations. Classical traveltime tomography can retrieve the large velocity and reflector structures, while prestack statistical tomography estimates by a direct formula the transverse covariance structure of small-scale velocity heterogeneities. In seismic reflection cases,

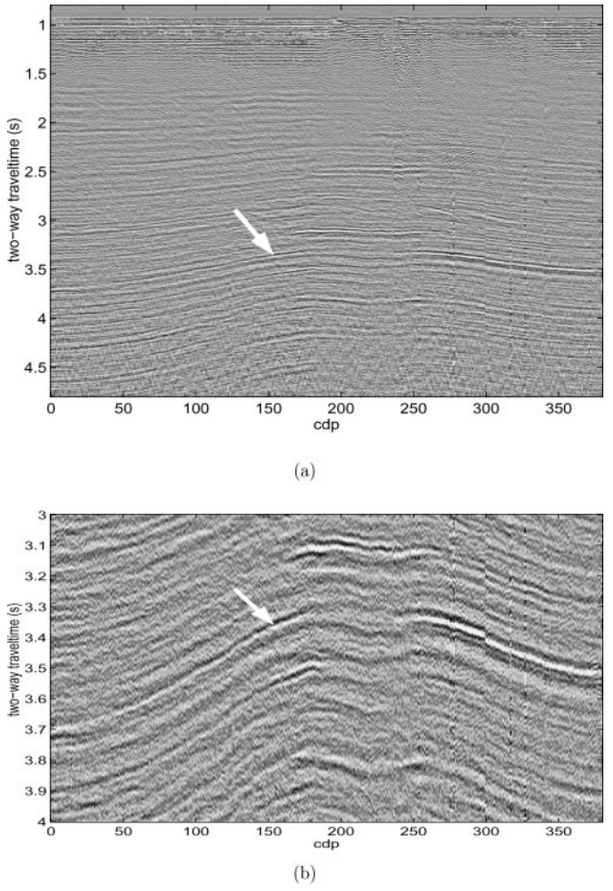

FIG. 11. (a) Prestack seismic section (offset $x = 350$ m) in the time domain (in seconds). The white arrow shows the picked reflector. (b) Zoom on the picked reflector (in seconds).

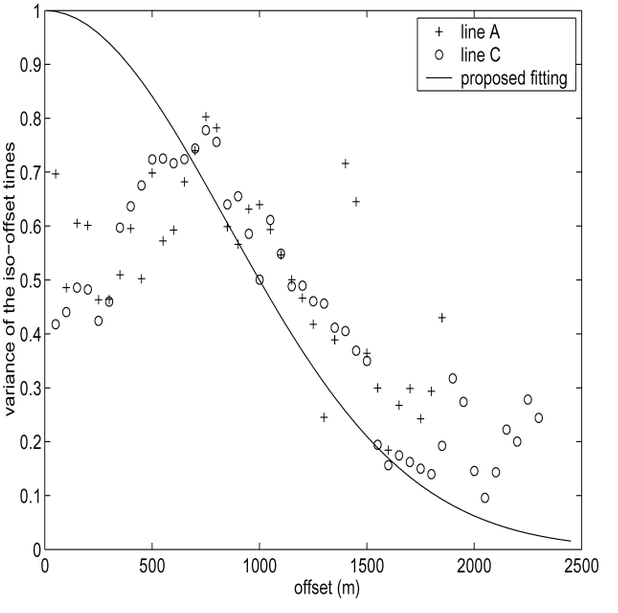

FIG. 12. Normalized variance of the iso-offset traveltime collections for acquisition lines A and C. The proposed curve fit is calculated with $a = 1200$ m for the horizontal correlation length of the velocity field.

using only the traveltimes with small offsets suppresses the problem of rapid reflector fluctuations. The second method, poststack traveltime tomography, is a manual curve-fitting procedure (Geraets and Galli, 2002) and is therefore more difficult to apply. However, it is based on the use of the spatial covariance of stacking velocities and hence does not require any prestack picking. For users, we present two flowcharts, one for each method, describing the steps in the algorithm.

First, for prestack statistical tomography the steps are as follows.

1) Pick traveltimes $T_{\mathbf{m}}(x)$ at different offsets x for a selected horizon from prestack seismic data ($\mathbf{m}$ is the midpoint).
2) Perform traditional methods (velocity analysis, traveltime tomography, . . .) to obtain a smooth velocity macromodel.
3) Compute the traveltimes $T_{0\mathbf{m}}(x)$ for the smooth model and obtain the relative traveltime fluctuations $\tau(x) = T_{\mathbf{m}}(x)/T_{0\mathbf{m}}(x)$.
4) Compute the experimentally observed variance of $\tau(x)$ for each offset x and fit it with a smooth polynomial function. This is done for ease of differentiation and integration in the following step. Fitting the initial part of the curve and its initial slope is more important than fitting the curve at large lags.
5) Use equations (25) and (26) to find the spatial covariance of the velocity heterogeneities.

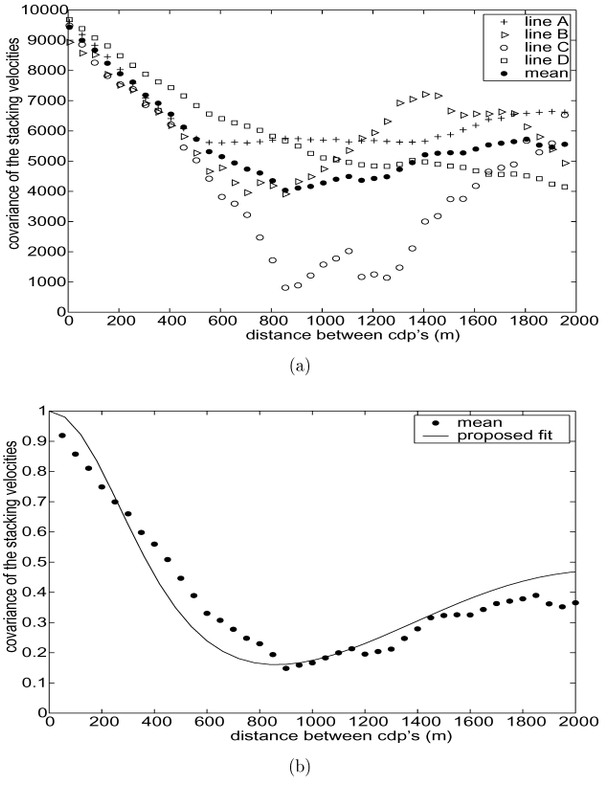

FIG. 13. (a) Stacking velocity covariances [in $(m/s)^2$] for the four different lines and the calculated mean. (b) Mean normalized covariance of the stacking velocities and its proposed fit.

Second, the poststack approach consists of iterative fitting of observed stacking velocity covariance to the theoretically predicted covariance from equation (33). The steps are as follows.

1) Perform velocity analysis and obtain a stacking velocity profile along a CDP line at the horizon of interest.
2) Compute the experimentally observed covariance of the stacking velocity.
3) Start with an initial guess model for the instantaneous velocity fluctuations, and compute the covariances for traveltimes and squares of traveltimes. This involves using equations (C-2), (C-3), (C-4), and (34).
4) From the covariance of the squared traveltimes and the source–receiver geometries, compute the theoretical covariance model for stacking velocity using equations (33) and (35).
5) Compare the predicted covariance with the observed covariance. Reduce the misfit by iteratively looping through the steps after perturbing the parameters of the covariance model for the velocity fluctations. Fit the first zero crossing of the observed stacking velocity covariance curve.

The 2D numerical examples are performed on synthetic random media. For the prestack and poststack algorithms, seismic reflection experiments in random media with idealized covariance show good estimates (errors <20%) of the horizontal correlation length of velocity heterogeneities. In a geologically realistic medium (nonstationary), we demonstrate the practicability of the prestack inversion of the correlation lengths transverse to the wave propagation direction (errors of 20%). Last, we present an application to real data. In this case, the prestack traveltime picking is difficult, and the prestack statistical tomography is sensitive to this process. It is efficiently replaced by the less precise (in easy cases) but more robust (in real cases) poststack statistical tomography.

For clarity, we used a very simple model in this article. Following the same developments, it is easy to obtain multilayer versions of the results exposed, some of which are already presented in the literature (Touati, 1996; Iooss, 1998b). To be closer to real media, Geraets et al. (2002) include a vertical gradient of the velocity field in their modeling. However, for such realistic models, it is generally impossible to find equivalent forms of equation (15), using the Abel transform to give an explicit expression of the horizontal correlation length.

The inversions addressed in this paper are valid for obtaining scales of stochastic heterogeneities that are larger than the wavelength and that have an impact on traveltimes. Some works, based on multiple scattering theory (amplitude attenuation and generation of codas), try to furnish inversion algorithms for stochastic heterogeneities with scales smaller than the wavelength (Van der Baan, 1999). The determination of all of these statistical scales can be a very useful input for better modeling the internal architecture of reservoirs and aquifers.

ACKNOWLEDGMENTS

This work was supported by the Centre de Géostatistique of the École des Mines de Paris, with the financial support of ENI-Agip division. T. M. was supported by the Stanford Rock Physics Project. We acknowledge P. Ruffo for helpful discussions and for providing the real data set. Also, we are grateful

to A. Ehinger and the KIM team of the Institut Français du Pétrole for allowing the use of their traveltime tomography software. Thanks to P. Podvin for his eikonal resolution code and to C. Lantuéjoul for his random media simulation program. This work was greatly improved by the remarks of P. Thore and an anonymous reviewer.

REFERENCES

Aki, K., 1973, Scattering of P waves under the Montana LASA: J. Geophys. Res., **78**, No. 8, 1334–1346.

Bishop, T. N., Bube, K. P., Cutler, R. T., Langan, R. T., Love, P. L., Resnick, J. R., Shuey, R. T., Spindler, D. A., and Wyld, H. W., 1985, Tomographic determination of velocity and depth in laterally varying media: Geophysics, **50**, 903–973.

Chernov, L. A., 1960, Wave propagation in a random medium: McGraw-Hill Book Company.

Chilès, J. P., and Delfiner, P., 1999, Geostatistics: Modeling spatial uncertainty: John Wiley & Sons, Inc.

Chu, J., Xu, W., and Journel, A. G., 1994, 3-D implementation of geostatistical analyses, the Amoco case study, *in* Yarus, J., and Chambers, R., Eds., Stochastic modelling and geostatistics; principles, methods and case studies: AAPG Comp. Appl. Geol., **3**, 201–217.

Claerbout, J. F., 1985, Imaging the earth's interior: Blackwell Scienctific Publication, Inc.

Delprat-Jannaud, F., and Lailly, P., 1993, Ill-posed and well-posed formulation of the reflection travel time tomography problem: J. Geophys. Res., **98**, 6589–6605.

Deutsch, C. V., and Journel, A. G., 1992, Gslib: Geostatistical software library and user's guide: Oxford Univ. Press.

Flatté, S. M., and Wu, R. S., 1988, Small-scale structure in the lithosphere and asthenosphere deduced from arrival time and amplitude fluctuations at NORSAR: J. Geophys. Res., **93**, No. B6, 6601–6614.

Geraets, D., and Galli, A., 2002, Statistical traveltime tomography in terms of stacking velocity: Pure Appl. Geophys., **159**, 1617–1636.

Geraets, D., Galli, A., and Ruffo, P., 2002, Estimating the covariance of a velocity field accounting for a linear vertical gradient: 64th Conf. & Exhib. Eur. Assn. Geol. Eng., Abstracts, C32.

Geraets, D., Galli, A., Ruffo, P., and Rossa, E. D., 2001, Instantaneous velocity field characterization through stacking velocity variography: 71st Ann. Internat. Conf., Soc. Expl. Geophys., Expanded Abstracts.

Gibson, B. S., and Levander, A. R., 1990, Apparent layering in common-midpoint stacked images of two-dimensionally heterogeneous targets: Geophysics, **55**, 1466–1477.

Gold, N., Shapiro, S. A., Bojinski, S., and Müller, T. M., 2000, An approach to upscaling for seismic waves in statistically isotropic heterogeneous elastic media: Geophysics, **65**, 1837–1850.

Han, D., 1986, Effects of porosity and clay content on acoustic properties of sandstones and unconsolidated sediments: Ph.D. dissertation, Stanford Univ.

Inoue, H., 1986, A least-squares smooth fitting for irregularly spaced data: Finite element approach using the cubic b-spline basis: Geophysics, **51**, 2051–2066.

Iooss, B., 1998a, Seismic reflection traveltimes in two-dimensional statistically anisotropic random media: Geophys. J. Internat., **135**, 999–1010.

——— 1998b, Tomographie statistique en sismique réflexion: Estimation d'un modèle de vitesse stochastique: Thesis, École des Mines de Paris.

Iooss, B., and Galli, A., 2000, Statistical tomography for seismic reflection data: 6th Internat. Geostat. Congress, Geostatist. Ass. Southern Africa, Proceedings, CD-ROM.

Iooss, B., and Samuelides, Y., 1998, Inversion of velocity statistical parameters from traveltimes: 135th Mtg., Acoust. Soc. Am., Proceedings, 2319–2320.

Iooss, B., Blanc-Benon, P., and Lhuillier, C., 2000, Statistical moments of travel times at second order in isotropic and anisotropic random media: Waves in Random Media, **10**, 381–394.

Jurado, F., Lailly, P., and Ehinger, A., 1998, Fast 3D two-point raytracing for traveltime tomography: Math. Methods Geophys. Imaging, SPIE, Proceedings, **V**, 70–81.

Klimeš, L., 2002a, Application of the medium covariance functions to travel-time tomography: Pure Appl. Geophys., **159**, 1791–1810.

——— 2002b, Estimating the correlation function of a self-affine random medium: Pure Appl. Geophys., **159**, 1833–1854.

Lantuéjoul, C., 1994, Non conditional simulation of stationary isotropic multigaussian random function, *in* Armstrong, M., and Dowd, P. A., Eds., Geostatistical simulations: Kluwer, 147–177.

Matheron, G., 1973, The intrisic random functions and their application: Adv. in Appl. Prob., **5**, 439–468.

——— 1991, Géodésiques aléatoires, *in* Les Cahiers de Géostatistique: Ecole des Mines de Paris, **1**, 1–18.

Mukerji, T., Mavko, G., Mujica, D., and Lucet, N., 1995, Scale-dependent seismic velocity in heterogeneous media: Geophysics, **60**, 1222–1233.

Müller, G., Roth, M., and Korn, M., 1992, Seismic-wave traveltimes in random media: Geophys. J. Internat., **110**, 29–41.

Podvin, P., and Lecomte, I., 1991, Finite difference computation of traveltimes in very contrasted velocity models: A massively parallel approach and its associated tools: Geophys. J. Internat., **105**, 271–284.

Roth, M., 1997, Statistical interpretation of traveltime fluctuations: Phys. Earth Plan. Int., **104**, 213–228.

Rubin, Y., Mavko, G., and Harris, J., 1992, Mapping permeability in heterogeneous aquifers using hydrologic and seismic data: Water Resources Res., **28**, 1809–1816.

Rytov, S. M., Kravstov, Y. A., and Tatarskii, V. I., 1987, Principles of statistical radiophysics: Springer-Verlag.

Samuelides, Y., 1998, Velocity shift using the Rytov approximation: J. Acoust. Soc. Am., **104**, 2596–2603.

Samuelides, Y., and Mukerji, T., 1998, Velocity shift in heterogeneous media with anisotropic spatial correlation: Geophys. J. Internat., **134**, 778–786.

Sato, H., and Fehler, M. C., 1998, Seismic wave propagation and scattering in the heterogeneous earth: Springer Pub. Co., Inc.

Scales, J., and Tenorio, L., 2001, Prior information and uncertainty in inverse problems: Geophysics, **66**, 389–397.

Shapiro, S., and Kneib, G., 1993, Seismic attenuation by scattering: Theory and numerical results: Geophys. J. Internat., **114**, 373–391.

Tarantola, A., 1987, Inverse problem theory: Methods for data fitting and model parameter estimation: Elsevier Science Publ. Co., Inc.

Thore, P. D., and Juliard, C., 1999, Fresnel-zone effect on seismic velocity resolution: Geophysics, **64**, 593–603.

Touati, M., 1996, Contribution géostatistique au traitement de données sismiques: Thesis, Ecole des Mines de Paris.

Touati, M., Iooss, B., and Galli, A., 1999, Quantitative control of migration: A geostatistical attempt: Math. Geol., **31**, 277–295.

Tyler, N., and Finley, R. J., 1991, Architectural controls on the recovery of hydrocarbons from sandstone reservoirs, *in* Miall, A. D., and Tyler, N., Eds., The three-dimensional facies architecture of terrigenous clastic sediments and its implications for hydrocarbon discovery and recovery: Soc. Expl. Paleont. Mineral.

Van der Baan, M., 1999, Deux méthodes d'inférence statistique appliquées aux données de sismique réflexion profonde: Détection de signaux et localisation d'ondes: Thesis, Univ. de Grenoble.

Williamson, P. R., and Worthington, M. H., 1993, Resolution limits in ray tomography due to wave behavior: Numerical experiments: Geophysics, **58**, 727–735.

Wook, B. L., and Wenlong, X., 2000, 3-D geostatistical velocity modelling: Salt imaging in a geopressured environment: The Leading Edge, **19**, 32–36.

Wu, R. S., and Flatté, S. M., 1990, Transmission fluctuations across an array and heterogeneities in the crust and upper mantle: Pure Appl. Geophys., **132**, 175–196.

APPENDIX A
DIRECT INVERSION OF VELOCITY COVARIANCE

We want to invert equation (13). Starting from the function

$$I(x) = \frac{\partial}{\partial x}[xC_\tau(x, L)], \tag{A-1}$$

we have, using equation (3),

$$\begin{aligned} I(x) &= \frac{2\sigma_\epsilon^2}{L}\int_0^{+\infty} N(x, z)\, dz \\ &= \frac{2\sigma_\epsilon^2}{L}\int_0^{+\infty} C_\epsilon\left(\sqrt{\frac{x^2+\Lambda^2 z^2}{a^2}}\right) dz \quad \text{(A-2)} \\ &= \frac{2\sigma_\epsilon^2}{L\Lambda}\int_x^{+\infty} C_\epsilon\left(\frac{r}{a}\right)\frac{r}{\sqrt{r^2-x^2}}\, dr, \quad \text{(A-3)} \end{aligned}$$

where $\Lambda = a/b$ is the anisotropy ratio.

Equation (A-3) can be transformed into an Abel integral equation whose solution is (Müller et al., 1992)

$$C_\epsilon\left(\frac{r}{a}\right) = -\frac{\Lambda L}{\pi\sigma_\epsilon^2}\int_r^{+\infty} \frac{\dfrac{\partial I(x)}{\partial x}}{\sqrt{x^2-r^2}}\, dx. \tag{A-4}$$

Since $C_\epsilon(0) = 1$, we deduce

$$C_\epsilon\left(\frac{r}{a}\right) = \frac{\left[\displaystyle\int_r^{+\infty} \frac{\dfrac{\partial I(x)}{\partial x}}{\sqrt{x^2-r^2}}\, dx\right]}{\left[\displaystyle\int_0^{+\infty} \frac{\dfrac{\partial I(x)}{\partial x}}{x}\, dx\right]}. \tag{A-5}$$

APPENDIX B
COVARIANCE OF STACKING VELOCITIES

Here we present how the covariance of the stacking velocities can be expressed as a function of the covariance of the square of the arrival times, following Geraets et al. (2001). Using a hyperbolic fit for the arrival times at one CDP α, the stacking velocity can be approximated by

$$V_{st\alpha} = \sqrt{\frac{n\displaystyle\sum_{i=1}^n x_i^4 - \sum_{i=1}^n x_i^2 \sum_{i=1}^n x_i^2}{n\displaystyle\sum_{i=1}^n T_{\alpha i}^2 x_i^2 - \sum_{i=1}^n T_{\alpha i}^2 \sum_{i=1}^n x_i^2}}$$

$$= \sqrt{\frac{n\displaystyle\sum_{i=1}^n x_i^4 - \sum_{i=1}^n x_i^2 \sum_{i=1}^n x_i^2}{n\displaystyle\sum_{i=1}^n T_{0\alpha i}^2 x_i^2 - \sum_{i=1}^n T_{0\alpha i}^2 \sum_{i=1}^n x_i^2 + n\sum_{i=1}^n T_{1\alpha i}^2 x_i^2 - \sum_{i=1}^n T_{1\alpha i}^2 \sum_{i=1}^n x_i^2}},$$

with x_i the offset of the ith receiver, n the amount of receivers used for the velocity analysis, and $T_{0\alpha i}$ and $T_{1\alpha i}$ the zero- and first-order terms of the expression of the traveltime $T_{\alpha i}$ (from the source, reflecting at the CDP α and recorded at the receiver i). At the first order, this is equivalent to

$$V_{st} \simeq \left(1 - \frac{c_0^2}{2}\left[\frac{n\displaystyle\sum_{i=1}^n T_{1\alpha i}^2 x_i^2 - \sum_{i=1}^n T_{1\alpha i}^2 \sum_{i=1}^n x_i^2}{n\displaystyle\sum_{i=1}^n x_i^4 - \left(\sum_{i=1}^n x^2\right)^2}\right]\right). \tag{B-1}$$

Expression (B-1) can be used in the covariance of the stacking velocities $V_{st\alpha}$ and $V_{st\beta}$, corresponding to two CDPs, α and β:

$$\begin{aligned} &cov(V_{st\alpha}, V_{st\beta}) \\ &\simeq c_0^2 cov\left(1 - \frac{c_0^2}{2}\frac{n\displaystyle\sum_{i=1}^n T_{1\alpha i}^2 x_i^2 - \sum_{i=1}^n T_{1\alpha i}^2 \sum_{i=1}^n x_i^2}{n\displaystyle\sum_{i=1}^n x_i^4 - \left(\sum_{i=1}^n x_i^2\right)^2},\right. \\ &\qquad \left. 1 - \frac{c_0^2}{2}\frac{n\displaystyle\sum_{j=1}^n T_{1\beta j}^2 x_j^2 - \sum_{j=1}^n T_{1\beta j}^2 \sum_{j=1}^n x_j^2}{n\displaystyle\sum_{j=1}^n x_j^4 - \left(\sum_{j=1}^n x^2\right)^2}\right) \\ &= \frac{c_0^6}{4}\sum_{i=1}^n\sum_{j=1}^n k(i, j, n) cov\left(T_{\alpha i}^2, T_{\beta j}^2\right), \end{aligned} \tag{B-2}$$

where $k(i, j, n)$ is a function of the layout

$$k(i,j,n)=\frac{n^2x_i^2x_j^2-nx_j^2\left(\sum_{k=1}^{n}x_k^2\right)-nx_i^2\left(\sum_{k=1}^{n}x_k^2\right)+\left(\sum_{k=1}^{n}x_k^2\right)\left(\sum_{k=1}^{n}x_k^2\right)}{\left[n\sum_{k=1}^{n}x_k^4-\left(\sum_{k=1}^{n}x_k^2\right)\left(\sum_{k=1}^{n}x_k^2\right)\right]^2}.$$

APPENDIX C
COVARIANCE OF REFLECTION TRAVELTIMES

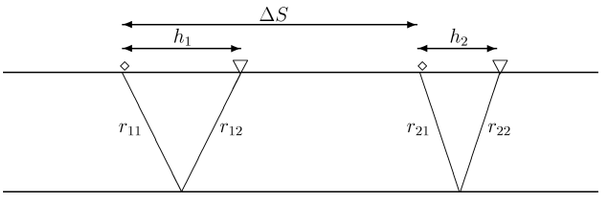

FIG. C-1. Scheme of the lay-out: ΔS is the distance between two sources; h_1 and h_2 are two offsets; r_{11} and r_{21} are the downgoing rays while r_{12} and r_{22} are the upgoing rays.

In "Inversion of prestack traveltimes," we compute the traveltime variance reflecting on an interface of depth L for an offset x. Let us consider two different shots, with sources S_1 and S_2 (separated by a distance ΔS) and offsets h_1 and h_2. We express the covariance of their reflecting traveltimes in terms of the standardized covariance $C_\epsilon(h)$. The layout we consider is illustrated in Figure C-1. The covariance can be expressed easily as

$$\begin{aligned}cov[T(\mathbf{r}_1),T(\mathbf{r}_2)]&=cov[T(\mathbf{r}_{11}),T(\mathbf{r}_{21})]\\&+cov[T(\mathbf{r}_{12}),T(\mathbf{r}_{21})]+cov[T(\mathbf{r}_{11}),T(\mathbf{r}_{22})]\\&+cov[T(\mathbf{r}_{12}),T(\mathbf{r}_{22})],\end{aligned}\tag{C-1}$$

where the four terms correspond to the mathematical expectation of the integral of the perturbation along the rays, as given by equation (10). In the case $S_1=S_2$ and $h_1=h_2$, we come back to the expression of the variance of the traveltimes given in equation (22).

Using geometrical laws and the Chernov approximation [equation (13)], it is possible to simplify equation (C-1) to obtain a fast computation of the traveltime covariance (Geraets amd Galli, 2002):

$$\begin{aligned}cov[T(\mathbf{r}_1),T(\mathbf{r}_2)]&=\frac{1}{c_0(\mathbf{r}_1)c_0(\mathbf{r}_2)}\\&\iint_{\mathcal{D}}\left[C_\epsilon\left(\Delta S+u\frac{-h_2-h_1}{2L}+v\frac{-h_1+h_2}{2L},2u\right)\right.\\&+C_\epsilon\left(\Delta S-h_1+u\frac{h_1-h_2}{2L}+v\frac{h_2+h_1}{2L},2u\right)\\&+C_\epsilon\left(\Delta S+h_2+u\frac{h_2-h_1}{2L}+v\frac{-h_1-h_2}{2L},2u\right)\\&\left.+C_\epsilon\left(\Delta S-h_1+h_2+u\frac{h_2+h_1}{2L}+v\frac{h_1-h_2}{2L},2u\right)\right]\\&\times 2dudv,\end{aligned}\tag{C-2}$$

with

$$\iint_{\mathcal{D}}dudv=\int_0^{L/2}dv\int_{-v}^{v}du+\int_{L/2}^{L}dv\int_{v-L}^{L-v}du.$$

We can approximate these four integrals with four terms of the form

$$\int_0^L\int_{-\infty}^{\infty}C_\epsilon(a_{0i}+a_{vi}v+a_{ui}u,2u)dudv,$$

with a_{0i}, a_{ui} and $a_{vi}(i=1,\ldots,4)$ functions of h_1, h_2, ΔS, and L.

Let us call min_i and max_i the minimum and maximum of $(|x_{1i}|,|x_{2i}|)$, defined as

$$\begin{cases}x_{1i}=\dfrac{2a_{0i}}{\sqrt{4a^2+a_{ui}^2b^2}},\\[2ex] x_{2i}=\dfrac{2a_{0i}+2a_{vi}L}{\sqrt{4a^2+a_{ui}^2b^2}}.\end{cases}\tag{C-3}$$

We can rewrite the four integrals $(i=1,\ldots,4)$ as

$$\begin{aligned}&\int_0^L\int_{-\infty}^{\infty}C_\epsilon(a_{0i}+a_{vi}v+a_{ui}u,2u)dudv\\&\quad=\frac{ab}{2a_{vi}}\int_{-\infty}^{\infty}\varphi(min_i,max_i,r)C_\epsilon(r)dr,\end{aligned}\tag{C-4}$$

where the term $\varphi(min_i,max_i,r)$ is equal to the sum of indicator functions ($\mathbb{1}_{[a,b]}(x)=1$ if $x\in[a,b]$ and 0 otherwise):

$$\varphi(m,M,r)=\begin{cases}\mathbb{1}_{[m,M]}\left[\dfrac{\pi}{2}-\sin^{-1}\left(\dfrac{m}{r}\right)\right]+\mathbb{1}_{[M,\infty]}\left[\sin^{-1}\left(\dfrac{M}{r}\right)-\sin^{-1}\left(\dfrac{m}{r}\right)\right] \text{ if } x_{1i}x_{2i}>0,\\[2ex] \mathbb{1}_{[0,m]}[\pi]+\mathbb{1}_{[m,M]}\left[\dfrac{\pi}{2}+\sin^{-1}\left(\dfrac{m}{r}\right)\right]+\mathbb{1}_{[M,\infty]}\left[\sin^{-1}\left(\dfrac{M}{r}\right)+\sin^{-1}\left(\dfrac{m}{r}\right)\right] \text{ otherwise.}\end{cases}$$